Draft version March 24, 2017
Typeset using LaTeX **twocolumn** style in AASTeX61

TECHNIQUES FOR HIGH CONTRAST IMAGING IN MULTI-STAR SYSTEMS II: MULTI-STAR WAVEFRONT CONTROL

D. Sirbu,[1] S. Thomas,[2] and R. Belikov[1]

[1] *NASA Ames Research Center, Moffett Field, Mountain View, CA, 94035*
[2] *Large Synoptic Survey Telescope, Tucson, Arizona 85719*

ABSTRACT

Direct imaging of exoplanets represents a challenge for astronomical instrumentation due to the high-contrast ratio and small angular separation between the host star and the faint planet. Multi-star systems pose additional challenges for coronagraphic instruments because of the diffraction and aberration leakage introduced by the additional stars, and as a result are not planned to be on direct imaging target lists. Multi-star wavefront control (MSWC) is a technique that uses a coronagraphic instrument's deformable mirror (DM) to create high-contrast regions in the focal plane in the presence of multiple stars. Our previous paper introduced the Super-Nyquist Wavefront Control (SNWC) technique that uses a diffraction grating to enable the DM to generate high-contrast regions beyond the nominal controllable region. These two techniques can be combined to generate high-contrast regions for multi-star systems at any angular separations. As a case study, a high-contrast wavefront control (WC) simulation that applies these techniques shows that the habitable region of the Alpha Centauri system can be imaged reaching 8×10^{-9} mean contrast in 10% broadband light in one-sided dark holes from 1.6-5.5 λ/D.

Keywords: direct imaging, high contrast, exoplanets, wavefront control, multi-star systems, binary stars, Alpha Centauri, deformable mirrors, coronagraph, Multi-Star Wavefront Control (MSWC), Super-Nyquist Wavefront Control (SNWC), Super-Nyquist Multi-Star wavefront control (SNMSWC)

1. INTRODUCTION

Radial velocity and transit surveys have confirmed more than 3000 exoplanets to date.[1] The *Kepler* mission and its follow-on *K2* have confirmed more than 2000 of these exoplanets including planets in the terrestrial regime. Due to the rich statistical data set provided by *Kepler* coupled with an understanding of its pipeline systematics, it has been possible to estimate that the occurrence rates of exoplanets between 1 and 2 Earth radii and within 1 AU of Sun-like stars (specifically GK dwarves) are relatively common (Burke et al. 2015). The next major step will be for direct imaging instruments to discover and characterize such exoplanets in the Sun's local neighborhood. Direct imaging of an exoplanet orbiting a single star represents a technical challenge because the contrast ratio between a Sun-like star and an Earth-sized rocky planet in the habitable zone is approximately ten orders of magnitude (Des Marais et al. 2002). Additionally, the angular separations typically require resolving capacity of around 100 milliarcseconds for direct imaging surveys within 30 parsec.

Ground-based instruments such as GPI (Macintosh et al. 2014), SPHERE (Beuzit et al. 2008), and SCExAO (Guyon et al., 2010) have already discovered and characterized exoplanets. These, however, have tended to be hot Jupiters with large orbital separations from their host star. Whereas ground-based direct imaging instruments can take advantage of larger apertures, achievable contrast is ultimately limited by the temporality of atmospheric turbulence. The coronagraphic instrument planned for the upcoming WFIRST (Shaklan et al. 2013) space mission will achieve deeper contrasts at smaller inner working angles. A direct imaging survey of dim, rocky planets in the habitable zone of Sun-like stars will likely be achieved only with a relatively-large aperture space telescope beyond WFIRST such as the current HabEx (Menneson et al. 2016) and LUVOIR (Bolcar et al. 2016) studies. Such instruments typically use a coronagraph to suppress stellar diffraction caused by the telescope's aperture and a wavefront control system using a deformable mirror (DM) to eliminate residual speckles formed by surface roughness and reflectivity variations across telescope optics. Laboratory testbeds have demonstrated deep contrast for different coronagraph architectures and telescope apertures and for small angular separations (Cady et al. 2016; Kern et al. 2016; Seo et al. 2016; Sirbu et al. 2016).

Currently envisioned ground and space-based instrument target lists contain only single star systems even though multi-star systems contain a majority of Sun-like stars in the solar neighborhood. Multi-star systems are not considered viable targets because, to date, instrumental approaches have provided means to deal only with the diffraction and aberration-induced leakage produced for the on-axis star. For a multi-star system, each off-axis star introduces additional diffraction and aberration-induced leakage (one exception being sufficiently wide multi-star systems for which the off-axis stars can be ignored). Alpha Centauri, the nearest star system to the Sun, is a prominent example of a star system not included in target lists for coronagraph instruments such as WFIRST, because the separation between the A and B components is only a few arcsec. Beyond dynamical multi-star systems, optical multi-star systems (consisting of a combination of foreground and background stars) also exhibit off-axis stellar leakage that may have to be controlled by the coronagraphic instrument.

The main contribution of this paper is to present, and demonstrate via simulated examples, a wavefront control technique that uses non-redundant modes on the DM to enable multi-star wavefront control (MSWC). In Section 2, we discuss in more detail the scientific discovery possibilities enabled by this technique, while in Section 3 we illustrate the challenges that MSWC helps overcome. Section 4 describes the MSWC technique, and as an implementation example we extend the formalism of the widely-used single star electric field conjugation (EFC) algorithm to the multi-star case. In an earlier companion paper (Thomas et al. 2015), the Super-Nyquist Wavefront Control (SNWC) technique was introduced. This technique enabling suppression of residual speckles beyond the nominal Nyquist controllable region is briefly reviewed in Section 5. A simulated case study in Section 6 shows applications of the MSWC and SNMSWC algorithms to a binary system such as the Alpha Centauri system under different conditions. As a baseline scenario, we compare traditional, single-star wavefront control with MSWC. We simulate operation of MSWC for broadband light. Finally, we demonstrate the combination of these two techniques to enable Super-Nyquist Multi-Star Wavefront Control (SNMSWC) for the Alpha Centauri at both small and large angular separations and with the dark hole located beyond the DM's Nyquist limit with respect to either one or both stars.

2. SCIENTIFIC MOTIVATION

Direct imaging of exoplanets is planned via a suite of ground-based and space-based instruments. These instruments will provide the opportunity to characterize a

[1] Data from *exoplanet.eu*, January 2017

large number of exoplanets going beyond the statistical census obtained via indirect detections. Additionally, direct imaging of exoplanets will provide a survey of the nearest planets in our solar neighborhood. Only a direct imaging instrument would be able to spectroscopically characterize these exoplanets allowing for better understanding of their atmospheric composition and seasonal variations.

The diameter of the imaging telescope aperture imposes a set of fundamental limitations on a direct imaging survey. One such limitation is due to the photon flux from the exoplanet. Rocky exoplanets in particular exhibit low flux, and therefore the target star list is limited in distance as faraway stars require long integration times. Additionally the habitable zone of faraway stars is challenging to image as angular separations decrease. As a result, the list of target stars available for a particular aperture size is limited. In addition, all close multi-star systems are by default excluded from current target lists for direct imaging observations even though these contain a majority of potential target stars. Space-based missions have limited apertures but because they are not limited by the atmospheric turbulence, they can achieve higher contrasts. These missions therefore tend to focus the search around Sun-like stars rather than dimmer M-dwarves. Alpha Centauri, the nearest star system, is one example of the type of systems that could be imaged with a small dedicated telescope with a 30-45 cm aperture size (Belikov et al. 2015). To emphasize the importance of surveying multi-star systems in the solar neighborhood, stellar surveys have indicated that a majority of stars are part of multi-star systems (Abt 1983). For example, 5 out of the nearest 7 stars are located in multi-star systems. Within 10pc of the Sun, there are 69 known FGK stars out of which 42 are located in known multi-star system. The prevalance of Sun-like stars in multi-star systems holds out to 25pc (Raghavan et al. 2010) and beyond (Tokovinin 2014).

Thus, a capability to directly image the circumstellar and circumbinary environments in multi-star systems could substantially increase the possible target star list for a given space telescope aperture. Table 1 summarizes a few of the prime Sun-like stars targets within 10pc which are, however, located in multi-star systems and for which the companion introduces off-axis starlight leakage limiting the achievable contrast. The latest known angular separations between the target star and its companion are given in arcsec and computed in equivalent units of λ/D for $\lambda = 650$nm and $D = 2.4$m (representative of WFIRST). Also shown is the contrast floor due to the off-axis star leakage resulting from $\lambda/20$ phase aberrations. For example, 70 Ophiucchi has two components with an angular separation of 6.5 arcseconds and a δV magnitude difference of 2.0. High-contrast imaging around 70 Ophiucchi A would be limited at a contrast floor of 1.9×10^{-7} because of the off-axis contribution from its close-in and bright companion 70 Ophiucchi B. 70 Ophiucchi B is a Sun-like star and a target of interest itself, but would be limited at a shallower contrast level of 7.9×10^{-7} due to 70 Ophiucchi A's off-axis starlight leakage contribution (which is the brighter component). 36 Ophiucchi is a triple star system, with the A and B components separated 5.1 arcseconds as and of similar visual magnitudes. The C component has a negligible leakage contribution being located beyond 700 arseconds from the AB pair. Close-in binaries such as Mu Cassiopeiae can also reach a contrast floor shallower than 10^{-10} even when the companion is a dim M-dwarf.

In Figure 1, the contrast floor induced by off-axis starlight leakage is shown for WFIRST. Out of 69 FGK stars within 10pc, the leakage due to an off-axis companion limits contrast at a level shallower than 10^{-10} for 35 stars. These stars would, by default, be excluded from WFIRST's target list.

There is, however, a question whether exoplanets are expected to be present in the dynamical environment of multi-star systems. A number of studies have addressed planet formation mechanisms in binary systems concluding that circumbinary planet formation is similar to formation around a single star and that circumstellar planet formation is also possible with restrictions on orbit inclinations (Quintana et al. 2007; Duchene, G. 2010). Another important consideration is the long-term dynamical stability of exoplanets in circumstellar orbits. Circumstellar dynamically stable regions have been shown to exist in theory (Holman & Wiegert 1999). Additionally, planets in multi-star systems have been confirmed with a tally of 19 circumbinary and 34 circumstellar exoplanets around mostly binary stars but also including two triple star systems (Bechter et al. 2014); a recent study of Kepler candidates has shown, however, that their occurrence rates appear to be lower around multi-star than single-star systems (Kraus et al. 2016). Thus, direct imaging in the circumstellar environment would provide additional data to inform planet formation theories for multi-star systems.

In Section 6 of this paper, we simulate a direct imaging scenario for the Alpha Centauri system, which at 1.3 pc away from the Sun is a compelling science target. Recently, a planet candidate with a minimum 1.3 Earth mass was discovered around Proxima Centauri (Anglada-Escude, G. et al. 2016), an M-dwarf star that is relatively wide (although likely dynamically bound) with respect to Alpha Centauri A and B (Wertheimer

Table 1. Sample multi-star systems within 10 pc with a Sun-like primary and a close-in companion. Last known angular separations are shown in units of arcseconds and λ/D (assuming $\lambda = 650$nm and $D = 2.4$m), and computed contrast floor due to the off-axis leakage from the stellar companion assuming $\lambda/20$ phase aberrations.

Target Star	Spectral Type	Dist. (pc)	Vmag	Comp. Ang. Sep (arcsec)	(λ/D)	Comp. ΔVmag	Off-Axis Leakage (Contrast Floor)	Comment
α Cen A	G2V	1.3	0.0	4	71.6	1.3	7.6e-07	
α Cen B	K1V	1.3	1.3	4	71.6	-1.3	6.7e-08	
70 Oph A	K0V	5.1	4.1	6.5	116.4	2.0	1.8e-08	
70 Oph B	K4V	5.1	6.1	6.5	116.4	-2.0	7.9e-07	
36 Oph A	K2V	5.5	5.1	5.1	91.3	0.0	1.9e-07	AB in Triple
36 Oph B	K1V	5.5	5.1	5.1	91.3	0.0	1.7e-07	AB in Triple
μ Cas A	K1V	7.6	5.2	1.1	19.7	5.4	7.8e-08	B is M-Dwarf
p Eri A	K2V	7.8	5.7	11.4	204.1	0.2	2.1e-08	
p Eri B	K2V	7.8	5.9	11.4	204.1	-0.2	2.8.9e-08	
μ Her A	G5IV	8.3	3.4	0.8	14.3	7.3	4.3e-08	B is M-Dwarf

& Laughlin 2006). The Alpha Centauri stars feature eccentric orbits with an 80 year period leading to stellar separations varying between 11-36 AU, and whose dynamically stable region has been studied (Quintana et al. 2002; Quarles & Lissauer 2016). The stability limits for the semi-major axes for a circumstellar exoplanet's orbit about Alpha Centauri A or B are 2.78 ± 0.65 AU and 2.49 ± 0.71 AU respectively. Additionally, the planetary orbits have the highest probability distribution in the plane of the binary with a maximum stable inclination of approximately 60°. These stability regions for the Alpha Centauri system encompass the potential habitable zones for both stars computed following the method in Kopparapu et al. (2013). Alpha Centauri A is a G-class star with a habitable zone spanning 0.9-2.2 AU, while Alpha Centauri B is a K-class star with a habitable zone spanning 0.6-1.3 AU.

Finally, the technique to directly image multi-star systems is not limited to dynamically-bound star systems. Indeed, a combination of foreground and background stars can form an optical multi-star system which would exhibit the same imaging challenges. The technique could reduce epoch restrictions on follow-up observations imposed by nearby background stars and the proper motion of a potential target star, and would enable imaging when background stars are not identifiable a priori (for example obscured by the diffraction halo of the target star). Out of 69 FGK stars within 10pc, 51 stars have a recorded companion even though only 42 stars are in multi-star systems. Thus, 9 FGK stars have optical companions.

3. MULTI-STAR IMAGING CHALLENGES

The challenge of direct imaging multiple star systems is augmented in comparison to a single star system since, in addition to the central star, light coming from one or more off-axis stars must also be suppressed. An option that has been proposed is to design a coronagraph that suppresses both the on-axis and off-axis stars (Cady et al. 2011). However, the off-axis coronagraph would only block diffraction from the off-axis star and speckles would still be present and require removal with a wavefront control system (Thomas et al. 2015). Thus, for a coronagraph to create a high-contrast region and image the circumstellar region of a multi-star system, a wavefront control solution is necessary, and depending on final contrast level requirements also sufficient to remove the light coming from the off-axis star. One exception to this discussion would be the case of a starshade blocking the off-axis starlight – since the occulter is external to the telescope in this configuration speckles from the off-axis star are no longer a limiting factor.

To illustrate the challenge of creating a high-contrast region for a multi-star system, refer to Figure 2 which represents a simple unobscured circular pupil featuring an on-axis and an off-axis star separated by 10 λ/D angular separation. Each star creates its own point spread function (PSF) in the telescope's focal plane, which are shown independently in the left and center panes of Figure 2. The intensity of the combined multi-star PSF shown in the corresponding right pane is formed by the incoherent addition of the individual stellar PSFs. The main contribution of this paper is to present in detail a

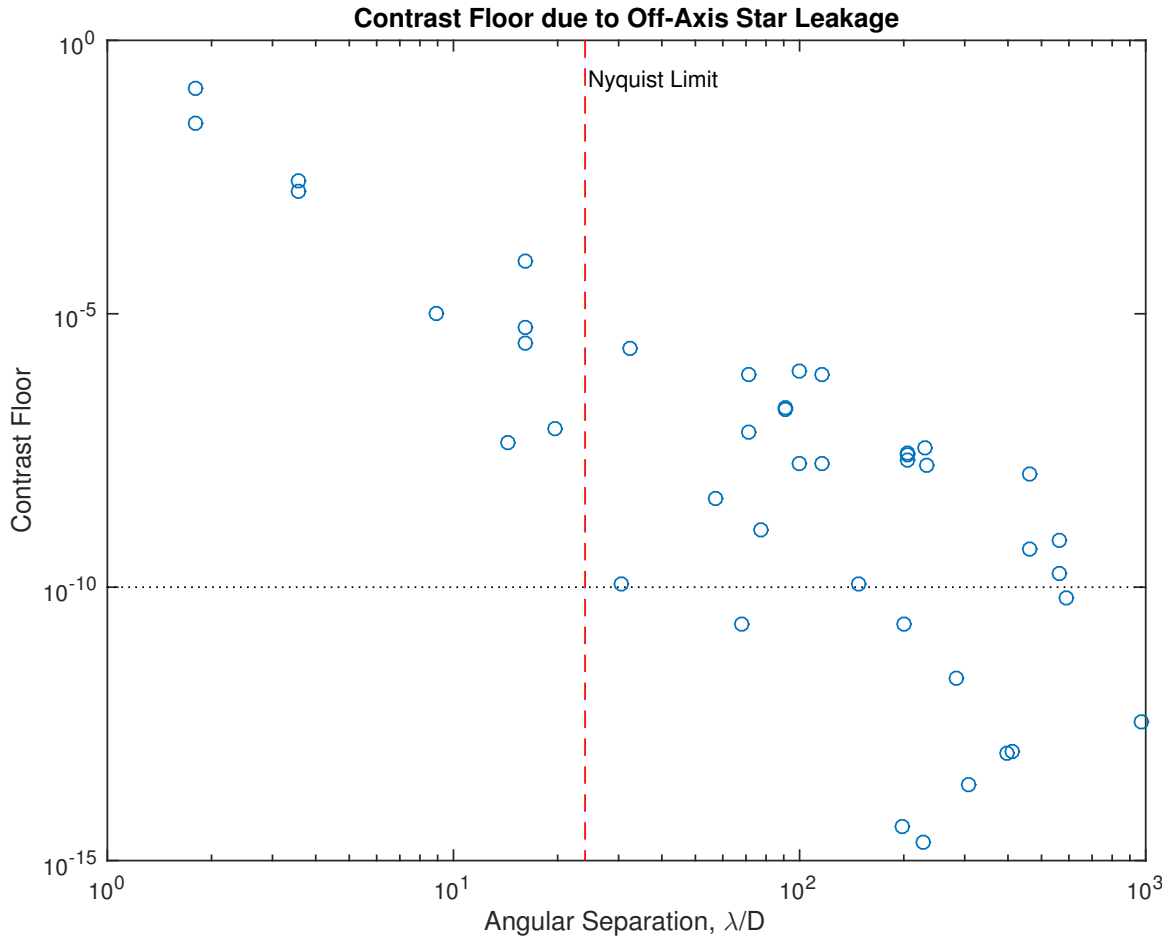

Figure 1. There are 69 FGK stars within 10pc. Assuming a $D = 2.4$m primary with $\lambda/20$ phase aberrations and $\lambda = 650$nm, the off-axis starlight from a companion introduces a contrast floor shallower than 10^{-10} for 35 of these stars. Shown also is the Nyquist limit for a 48×48 DM, with 10 stars at Sub-Nyquist angular separations.

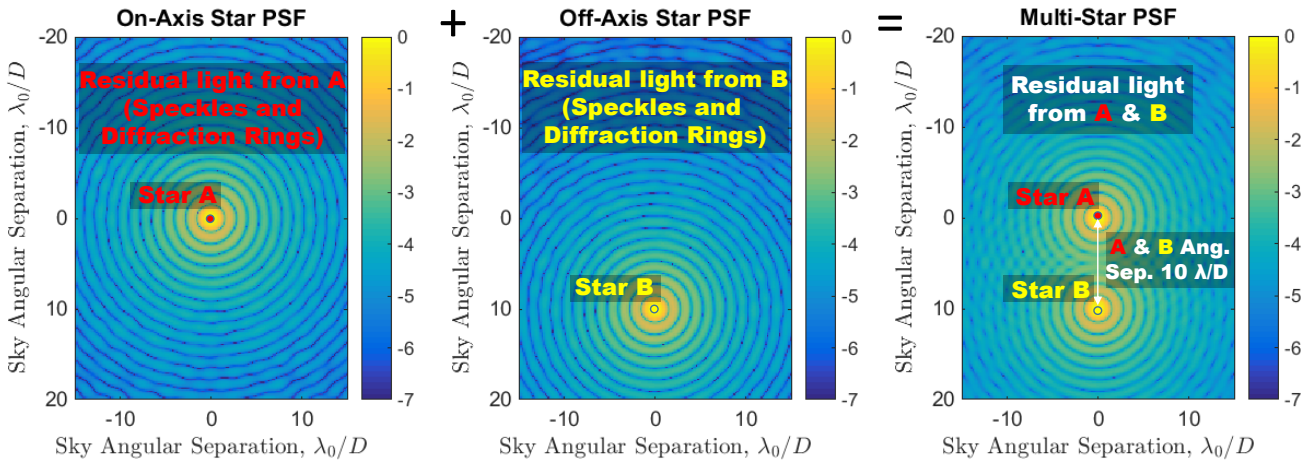

Figure 2. The multi-star PSF is the incoherent sum of the PSFs for each individual star. Thus, an off-axis star limits the achievable contrast in the dark hole to the level set by its own diffraction rings and aberration-induced speckles even if a DM is used to create a dark hole around the on-axis star.

multi-star wavefront control technique that can control leakage from both stars simultaneously in the desired dark hole region. This is then demonstrated in simulation for realistic dark hole geometries showing that deep contrast ratios can be obtained.

A separate challenge may arise due to the angular separation between the two stars. The particular restriction here is imposed by the number of actuators available on the DM. Traditionally, the outer working angle of the wavefront control system is given by the maximum controllable frequency of the DM (its Nyquist limit). If the desired dark hole is at an angular separation with respect to each of the stars that is within the Nyquist limit then a feasible region of high-contrast can be found that simultaneously suppresses both stars. However, for stars with wider angular separations or a larger telescope aperture it is likely that the dark hole is located beyond the controllable Nyquist-limit for one of the stars. In this case, MSWC can be combined with the Super-Nyquist Wavefront Control (SNWC) technique (Thomas et al. 2015) which allows using higher quilting orders introduced by a diffraction grating to replicate the PSF and extend the controllable spatial frequencies. As part of the specific case study in this paper, we will demonstrate how SNWC can be combined with MSWC to gain complete coverage of the dynamically stable region in which potential circumstellar exoplanets could exist in the Alpha Centauri system.

4. MULTI-STAR WAVEFRONT CONTROL

Several wavefront control techniques have been developed to eliminate residual diffraction leakage and speckles due to aberrations in the optical train for a single on-axis star. These techniques include Electric Field Conjugation (Give'on et al. 2007), Stroke Minimization (Pueyo et al. 2011), and traditional Speckle Nulling. These techniques can also be used for a single off-axis star. We discuss how these wavefront control techniques can be adapted for the case of a binary star system for which mutually incoherent speckles from each star overlap spatially and thus must be simultaneously controlled.

As an illustrative example, consider Figure 3 where two stars are imaged with an unobscured pupil and separated by 16 λ/D (Nyquist separation for a DM with 32 $\times$ 32 actuators). Suppose that the desired dark hole is to be generated within 0-8 λ/D near the on-axis star and between the two stars. This dark hole could be generated for the on-axis star by applying a linear combination of sinusoidal modes with 0-8 cycles per aperture (cpa). Conversely, the same dark hole for the off-axis star would be located between 8-16 λ/D; the dark hole could be generated for the off-axis star using a linear combination of sinusoidal modes of 8-16 cpa. These modes are non-redundant and can therefore be used to independently generate dark holes for each star. An outstanding issue is that higher order (nonlinear) effects generate residual speckles; however, these can be eliminated iteratively when operated in a closed-loop. The only requirement for this is to iterate sequentially between stars (for speckle-nulling) or to perform the wavefront control simultaneously for both stars (for model-based EFC-like algorithms) rather than completely generate one star's dark hole and then the second star's dark hole. Figure 2 shows the generated multi-star dark hole. The same DM setting obtained to simultaneously generate the multi-star dark hole in the right pane is maintained for illustrative purposes with only the on-axis and off-axis stars in the left and center panels. Thus, each star's dark hole is shown independently and their incoherent sum shows the resulting multi-star dark-hole. Since there is no coronagraph, the MSWC dark hole in this illustrative example is limited in terms of contrast depth close-in to the central star. A cost of using MSWC for this binary star scenario is that the maximum dark hole area for MSWC is a factor of two smaller than the maximum dark hole area for a single star.

The problem of reconstructing the electric field for each star separately can be solved using the classical DM probe pair method (Give'on et al. 2011), but with a modification in the form of modulating the region of interest for each star sequentially. In the dark hole only the speckles corresponding to each star are modulated by the DM when the corresponding spatial frequencies are applied. As a consequence of the non-redundance of the dark hole location, a different set of spatial frequency modes on the DM will modulate each star.

The classical single-star EFC algorithm (Give'on et al. 2007) can be easily reformulated to generate a multi-star dark hole following these principles. The final electric field in the science plane E_f is related to the DM electric field by the coronagraph's optical train which is abstracted as the linear operator $\mathcal{C}$:

$$E_f(u,v) = \mathcal{C}\left\{E_{\rm DM}(x,y)\right\} \tag{1}$$

where $E_{\rm DM}$ is the electric field immediately after the DM plane. Then, separating the electric field into the wavefront aberration and the DM surface and applying the linear approximation:

$$E_f(u,v) = \mathcal{C}\left\{Ae^{\alpha+i\beta}e^{i\phi}\right\} \tag{2}$$

$$\approx E_{\rm ab} + i\mathcal{C}\left\{A\phi\right\} \tag{3}$$

Where in the above $E_{\rm ab} = \mathcal{C}\left\{Ae^{\alpha+i\beta}\right\}$ is the aberrated electric field that must be corrected by the phase ϕ applied across the DM surface. The spatial frequencies in the focal plane that constitute the dark hole with respect to the on-axis star is represented by the set $S = \{(u, v)\}$. The linearized system response relating changes in the electric field in the science plane to individual actuator pokes is given by the matrix G with dimensions $n_{\rm im} \times n_{\rm act}$, where $n_{\rm im}$ represents the number of pixels in the dark hole and $n_{\rm act}$ the total number of actuators across DM. The individual actuator heights $\bar{a}$ must then satisfy the following equation to correct the aberrated electric field:

$$G\bar{a} = -E_{\rm ab} \tag{4}$$

Finding a solution to this equation for the DM actuator heights $\bar{a}$ represents classical EFC for a single star.

To extend for the case of MSWC, the set of pixels that forms the dark hole for each star must first be defined. For the nth star, $S_n = \{u - u_{*,n}, v - v_{*,n}\}$, with $u_{*,n}$ and $v_{*.n}$ the focal plane coordinates with respect to the on-axis star. The dark hole geometry must be chosen such that all pixels are at non-redundant spatial frequencies, meaning that for a coordinate pair $(a, b) \in S_i$, $(a, b) \notin S_j, \forall i \neq j$. The non-redundancy requirement means that for n stars, the maximum MSWC controllable area is a factor of $1/n$ of a single star's controllable area. The nominal G matrix can be augmented to include the linearized response for individual actuator pokes for each star (up to G_n for the nth star) with respect to the pixels inside the dark holes at non-redundant spatial frequencies and the corresponding sets of aberrated electric field contributions for each star (up to $E_{\rm ab,n}$ for the nth star):

$$\begin{bmatrix} G_1 \\ \vdots \\ G_n \end{bmatrix} \bar{a} = - \begin{bmatrix} E_{\rm ab,1} \\ \vdots \\ E_{\rm ab,n} \end{bmatrix} \tag{5}$$

Solving the above system of equations (usually overdetermined, and thus in the least-squares sense) for the unknown actuator response $\bar{a}$ yields the desired DM solution in the form of response. Note that this formulation is with a single DM and a monochromatic correction.

For broadband correction, the linearized system response matrices are computed at each desired correction wavelength (e.g., $G_1(\lambda_1), G_1(\lambda_2), G_1(\lambda_3)$. A linear system of equations is constructed by augmentation via pairing the wavelength-dependent system response matrix (e.g., $G_1(\lambda_1)$) with the wavelength-dependent corresponding aberrated electric field (e.g., $E_{\rm ab,1}(\lambda_1)$). Thus, a system of equations corresponding to broadband correction at three different wavelengths for a binary star system can be written as follows:

$$\begin{bmatrix} G_1(\lambda_1) \\ G_1(\lambda_2) \\ G_1(\lambda_3) \\ G_2(\lambda_1) \\ G_2(\lambda_2) \\ G_2(\lambda_3) \end{bmatrix} \bar{a} = - \begin{bmatrix} E_{\rm ab,1}(\lambda_1) \\ E_{\rm ab,1}(\lambda_2) \\ E_{\rm ab,1}(\lambda_3) \\ E_{\rm ab,2}(\lambda_1) \\ E_{\rm ab,2}(\lambda_2) \\ E_{\rm ab,2}(\lambda_3) \end{bmatrix} \tag{6}$$

5. SUPER-NYQUIST MULTI-STAR WAVEFRONT CONTROL

For stars at angular separations greater than the Nyquist frequency, MSWC alone may no longer be sufficient to create dark holes. This is because the dark regions for the off-axis star are outside the DM's controllable range. In this case, SNWC can be combined with MSWC to enable Super-Nyquist Multi-Star Wavefront Control (SNMSWC).

The combined SNMSWC technique is illustrated in Figure 4 for two stars separated by a distance of $70\lambda/D$. SNMSWC uses a diffraction grating (either in the form of already existing print-through and quilting patterns on the DM or an exteral grating such as a diffractive pupil (Bendek et al. 2013)) that creates replicas of the PSF at spatial frequencies beyond the Nyquist limit. In the left-pane of Figure 4 a desired dark hole is located within the Nyquist limit for the on-axis star. Using a 32 $\times$ 32 DM's print-through pattern and quilting, a diffraction grid can be observed at regular intervals of $\pm 32\lambda/D$ across the field of view. The central pane shows that the control region for the off-axis star is outside its Nyquist limit. To create a dark hole in that region it will be necessary to use the nearest replica PSF from the off-axis star's diffraction orders. This PSF replica enables modulating speckles of the off-axis star at 70 λ/D (at Super-Nyquist frequencies), and create a dark hole as shown. Finally, in the right pane the combined multi-star dark hole is shown with both the on-axis and off-axis stars simultaneously.

As discussed in the previous subsection for MSWC, to generate the dark hole simultaneously the dark hole region location must be non-redundant. For the SNMSWC example in Figure 4, this means that the dark hole must be non-redundant with respect to the on-axis star and the off-axis star's PSF replica.

6. SIMULATED CASE STUDY RESULTS

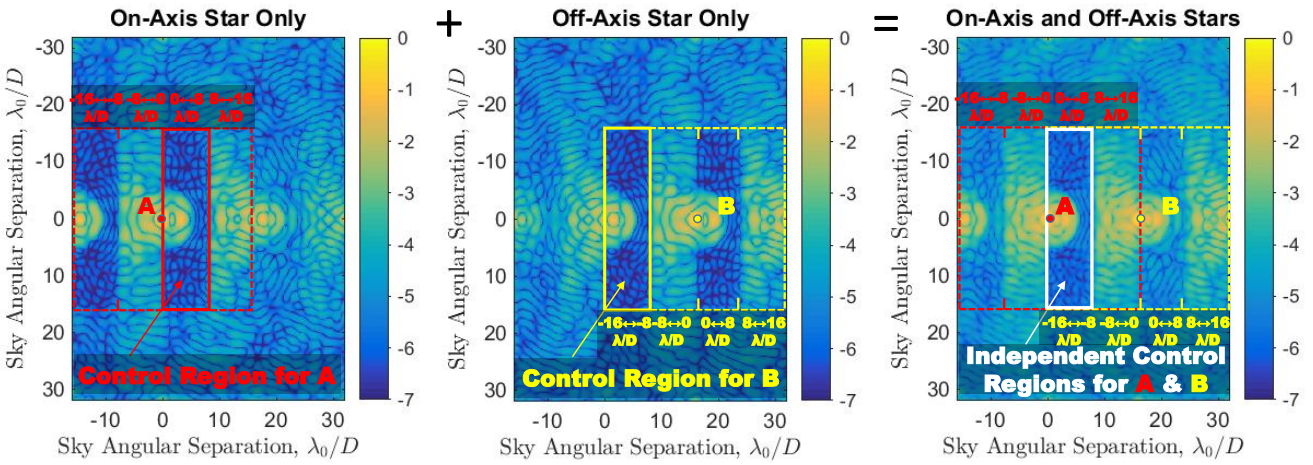

Figure 3. Simulation results of MSWC for an unobscured telescope pupil for a binary system with 16 λ/D angular separation between Stars A and B. Illustrated are the controllable regions with a 32 × 32 actuator DM for (*Left*) the on-axis star (A) and (*Center*) the off-axis star (B). (*Right*) The resulting multi-star feasible dark zone using non-redundant DM modes creating independent control regions for A and B.

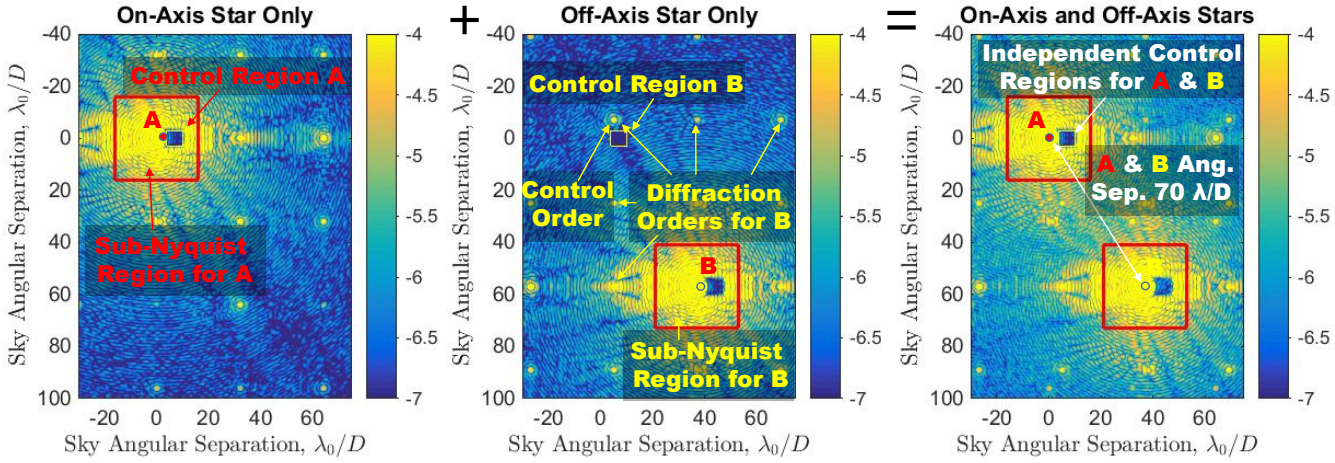

Figure 4. Simulation results of MSWC for an unobscured telescope pupil for a binary system with 70 λ/D angular separation between Stars A and B. The dark hole is located outside the Nyquist limit for the off-axis star (B) requiring combination with SNWC using a diffraction grating that generates a regular diffraction grating. Illustrated are the independent dark holes for the (*Left*) on-axis star (A), (*Center*) off-axis star (B), and (*Right*) combined multi-star (both on-axis and off-axis).

As a simulated demonstration of multi-star wavefront control, we explore a dark hole region of interest for a plausible configuration of the Alpha Centauri system. In Table 2, the angular separations of the Alpha Centauri A with respect to its binary companion B are shown for three epochs. Additionally, circumstellar habitable zones are computed for both Alpha Centauri A (a G-class star) and Alpha Centauri B (a K-class star) using stellar luminosity and temperature as input parameters (Kopparapu et al. 2013). Spanning the habitable zone out to the stability limit defines the region of interest that a dark zone should cover. This is of particular importance to determine the necessary inner working angle close-in to the target star. Angular separations are shown in units of λ/D for both a small telescope with an aperture of 0.35m (Belikov et al. 2015) and for a larger telescope such as WFIRST with an aperture of 2.4m at three different representative optical wavelengths. Due to its proximity, the Alpha Centauri system is particularly well-suited to observation with a small-class telescope with angular separations within the Nyquist limit for typical DM actuator counts, while wider binaries such as 61 Cygni would require SNMSWC. Conversely, for a larger aperture the Alpha Centauri system would

Table 2. Angular separations for Alpha Centauri AB and Mu Cassiopeiae A converted from units of arcsec to λ/D for both small and medium aperture telescopes (representative of ACESat and WFIRST with $D = 0.35$m and $D = 2.4$m respectively) at three distinct wavelengths ($\lambda_1 = 500$nm, $\lambda_2 = 650$nm, $\lambda_3 = 800$nm).

Target Star	Description	Ang. Sep.	Ang. Sep (D = 0.35m)			Ang. Sep (D = 2.4m)		
		(arcsec)	λ_1/D	λ_2/D	λ_3/D	λ_1/D	λ_2/D	λ_3/D
α Cen A	B Sep. (2021)	6	20.4	15.7	12.7	140	107	87.3
α Cen A	B Sep. (2022)	7	23.8	18.3	14.9	163	125	102
α Cen A	B Sep. (2023)	8	27.2	20.9	17.0	186	143	116
α Cen A	Inner HZ, 0.9 AU	0.7	2.36	1.81	1.47	16.2	12.4	10.1
α Cen A	Outer HZ, 2.2 AU	1.6	5.57	4.29	3.48	38.2	29.4	23.9
α Cen B	Inner HZ, 0.6 AU	0.4	1.39	1.07	0.87	9.55	7.35	5.97
α Cen B	Outer HZ, 1.3 AU	1.0	3.29	2.53	2.06	22.6	17.4	14.1
μ Cas A	B Sep. (2017)	1.0	3.39	2.61	2.12	23.27	17.9	14.5
μ Cas A	Inner HZ, 0.6 AU	0.08	0.28	0.22	0.18	1.94	1.50	1.21
μ Cas A	Outer HZ, 1.1 AU	0.15	0.50	0.38	0.31	3.42	2.63	2.14

require SNMSWC while other potential binary target stars such as the farther away Mu Cassiopeiae fall within the sub-Nyquist regime for typical DM actuator counts and its observation would be enabled by MSWC.

For this case study, we consider the 0.35m aperture telescope imaging the Alpha Centauri system at 650nm with a $17.5\lambda/D$ angular separation between the binary stars (corresponding to an epoch between 2021 and 2022 – see Table 2, and incidentally this separation is equally representative of Mu Cassiopeiae for a 2.4m aperture). The central star is assumed to be Alpha Centauri A which is a factor of three brighter than Alpha Centauri B. The dark hole is generated with a single DM featuring 32 x 32 actuators with a working angle between 1.6 λ/D and $5.5\lambda/D$ covering the entire habitable zone of Alpha Centauri A with the outer working angle going slightly beyond the ≈2.5 AU dynamical stability limit. The image plane resolution is set at 6 samples per λ/D. To enable a dark hole at deep raw contrasts sufficient to directly image dim, rocky planets a coronagraph blocking diffraction from the central star is necessary because of the close inner working angle operating near the first diffraction ring. A classical phase-induced amplitude apodization (PIAA) coronagraph (Guyon et al., 2003) in combination with an inverse PIAA (to recover a wide field of view after blocking the central star) is used in a Lyot-style configuration. The PIAA coronagraph is chosen because it is is well-suited for operating at small inner working angles (within a configuration similar to Sirbu et al. (2016)).

Notwithstanding the choice of PIAA coronagraph for this case study, the MSWC technique presented here is applicable to other coronagraph architectures as well.

6.1. *Baseline Case*

For this epoch and the 0.35m telescope aperture, a single-sided dark hole between $1.6 - 5.5\lambda/D$ is located between Alpha Centauri A and B, falling within the sub-Nyquist controllable regime for this DM configuration for both stars.

Before the wavefront control loop is applied, at 650nm and without a coronagraph the mean-contrast from the unaberrated on-axis star measures 7.1×10^{-3}. After introduction of the coronagraph, the on-axis star's contribution is controlled by two orders of magnitude (but still dominated by diffraction) with a mean contrast contribution of 1.9×10^{-5}. The off-axis star's leakage contribution is at the same level but dominated by $\lambda/20$ phase aberrations (generated with a frequency spectral envelope following a $1/f^{3/2}$ power law) with a mean contrast of 1.2×10^{-5}. The combined multi-star measured contrast is the summation of the two stars' contributions at 3.1×10^{-5}.

Single-star wavefront control. As a control case, we consider application of traditional, single-star, closed-loop EFC for the the on-axis star only starting from this initial contrast level. Alpha Centauri A is not directly visible as it is on-axis and blocked by the coronagraph, while Alpha Centauri B is off-axis and unaffected by the coronagraph after the forward PIAA optics are reversed by the inverse PIAA optics. The Nyquist region for the 32 x 32 actuator DM is shown with respect to Alpha Centauri A, with the entire dark zone at sub-Nyquist

frequencies. The DM cancels only the speckles of the on-axis star ignoring the incoherent speckles from the off-axis star. The final control region with both stars included is shown in the left pane of Figure 5, with a mean contrast of 5.4×10^{-5} inside the dark hole. The on-axis star leakage is controlled to a deep mean contrast level of 1.5×10^{-10}, but ultimately the contrast is limited by the uncontrolled off-axis star's leakage. In fact, we note that minimizing only the on-axis star leakage results in a worse contrast level inside the dark hole due to additional leakage from the off-axis star when compared to not performing any wavefront control iterations. This inability to generate a dark hole by removing speckles from the on-axis star alone underlines the necessity to control the leakage of both stars simultaneously using MSWC.

Multi-star wavefront control. To complete the baseline scenario, we consider application of closed-loop EFC using MSWC starting from the same initial contrast level. The dark hole is created using the same physical settings as the control case. The final multi-star dark hole is shown in the right pane of Figure 5, with the sub-Nyquist region around Alpha Centauri B clearly indicated. The dark hole for the multi-star case is clearly visible with the mean contrast measured across is 1.9×10^{-9}, with Alpha Centauri A's contribution being 3.2×10^{-10} and Alpha Centauri B's contribution being 1.6×10^{-9}. The Strehl Ratio of the central star is 0.92 for these DM settings, demonstrating that deep contrast can be obtained with a small impact upon the flux from a planet inside the dark hole.

6.2. *Broadband Case*

In the baseline scenario above, we optimized DM settings for monochromatic input light. In broadband, speckles are elongated radially and can leak additional light inside the dark zone if not specifically optimized across the entire broadband bandpass.

Monochromatic-optimized control. This situation can be observed in the left pane of Figure 6, where the same DM settings obtained under monochromatic light are maintained with broadband input light spanning a 10% bandpass about 650nm (generated at 1nm intervals between 617nm and 683nm). The mean contrast under these conditions degrades to 2.9×10^{-6}, nearly three orders of magnitude compared to the monochromatic case (right pane of Figure 5) for which these DM settings were specifically optimized for.

Broadband-optimized control. To counteract chromatic effects, the dark hole is generated by simultaneously optimizing the actuator heights of the DM for three evenly-spaced wavelengths inside this bandwidth: 626nm, 650nm, and 674nm. The corresponding broadband dark hole is shown in the right pane of Figure 7. The mean measured contrast for this 10% broadband multi-star dark hole is 8.3×10^{-9}, which represents an improvement of nearly two orders of magnitude compared to optimizing the settings monochromatically only (compare the left and right panes of Figure 7). As larger strokes on the DM are required for broadband optimization the Strehl Ratio of the central star is lower at 0.81. Nonetheless, this shows that MSWC can be operated in broadband with a very moderate loss of planet flux.

6.3. *Super-Nyquist Case*

For the epoch and telescope aperture example considered above, a single-sided dark hole located between Alpha Centauri A and B falls completely within the sub-Nyquist controllable regime for this DM configuration for both stars. Even when stars have a relatively close angular separation there may exist potential regions of interest of the focal plane that are at sub-Nyquist separations with respect to one star and at super-Nyquist separations with respect to the other star. Thus a dark hole could be either partially or fully at super-Nyquist separations with respect to the off-axis star. An even more general case occurs for stars with wide angular separations such that the entire sub-Nyquist region near the on-axis star may be super-Nyquist with respect to the off-axis star. A final case consists of a dark hole region of interest which is at super-Nyquist separations with respect to both stars.

Stars at small angular separations. The examples above for the epoch and small telescope aperture featured Alpha Centauri A and B relatively close with a 17.5 λ/D angular separation. All the example scenarios above considered fully sub-Nyquist multi-star wavefront control. For these cases, the single-sided dark hole is at 1.6-6 λ/D and located between Alpha Centauri A and B (the near-side dark hole). However, for this particular geometry a dark hole created on the opposite side of Alpha Centauri A (the far-side dark hole) lies within the Nyquist controllable limit with respect to Alpha Centauri A but outside the Nyquist controllable limit with respect to Alpha Centauri B. Thus, this geometry requires using SNWC in combination with MSWC to generate the dark hole in the required region of interest and obtain complete coverage of the habitable zone of Alpha Centauri A for this epoch.

To enable SNMSWC a grating must be introduced into the optical model (Thomas et al. 2015). Here, we consider a DM grating arising from the combined periodicity of the phase grating from the DM quilting pattern and the amplitude grating due to print-through arti-

facts – the grating model is obtained via interferometric images of a Boston Micromachines 32×32 DM and is detailed further in Sirbu et al. (2016b). The diffraction orders contain the replica PSFs of Alpha Centauri B and are located at $\pm 32\lambda/D$ intervals about the off-axis star. The first diffraction order used to modulate the speckles of Alpha Centauri B in the far-side dark zone is most clearly visible in the monochromatic PSF in the left pane of Figure 5. The peak of the PSF replica is located at -14.5 λ/D with respect to the on-axis star's location.

The final dark hole generated for a 10% bandwidth around 650nm on the far-side of Alpha Centauri A is shown in the left pane of Figure 7, shown with respect to the sub-Nyquist dark hole in the corresponding right pane for comparison. The dark hole has a mean contrast of 8.4×10^{-9} and a Strehl Ratio of the central star of 0.81. These results for the far-side dark hole (super-Nyquist with respect with respect to Alpha Centauri B) are consistent with the near-side dark hole (sub-Nyquist with respect to both Alpha Centauri A and B) and represent raw contrast without any form of post-processed speckle subtraction. Together, these results show that in principle it is possible to use a wavefront control system to generate a dark hole for a multi-star system. Additionally, these simulations have shown that the specific case of the Alpha Centauri system can be imaged with a small telescope aperture.

Stars at large angular separations. Next, we consider the case of a separation between the Alpha Centauri A and B for which MSWC wavefront control is not possible. Specifically, we consider the case of a 2.4m diameter telescope aperture. Thus, Alpha Centauri A and B are separated by 120 λ/D with the potential regions of interest spanning both sub-Nyquist and super-Nyquist separations with respect to the on-axis star (see Table 2). For all regions of interest around the on-axis star, the off-axis star is at super-Nyquist separations since it is located at a wide angular separation from the on-axis star.

Applying SNMSWC with the same DM grating model, we create a single-sided dark hole box located between $[7, 12]\,\lambda/D$ along the separation axis between the two stars and $[-6, 6]\,\lambda/D$ across the separation axis in monochromatic light at 650nm. This is shown in the left pane of Figure 8. The mean contrast achieved is 3.2×10^{-9} with a Strehl Ratio of 0.83.

Finally, we consider the case for which the dark hole is located at super-Nyquist separations with respect to both the on-axis and off-axis stars. For example, this is motivated by the fact that for a 2.4m diameter telescope the circumstellar habitable zone around Alpha Centauri A or B lies partially outside the Nyquist-controllable region with respect to the on-axis star. The right pane of Figure 8 features rectangular dark hole located between $[16, 22]\,\lambda/D$ along the separation axis between the two stars, and $[-5, 5]$ across the separation axis. Thus this region is outside both stars' Nyquist-controllable regions. SNMSWC is performed using the first diffraction order at $32\lambda/D$ for the on-axis star and the off-axis star's third-diffraction order located at $24\lambda/D$ with respect to the on-axis star. The mean contrast measured across the dark hole is 1.0×10^{-8} and the measured Strehl Ratio at 0.68.

7. CONCLUSIONS

A wavefront control technique that enables direct imaging of multi-star systems provides an opportunity to more than double the number of target stars in direct imaging surveys. Additionally, the Alpha Centauri system is such a binary system and the nearest star system and therefore provides a unique opportunity for direct imaging with a small telescope aperture from space.

In this paper, we have introduced a wavefront control technique that can be used with existing coronagraph instruments to enable the creation of non-redundant dark holes in which the circumstellar environment in multi-star systems can be surveyed for exoplanets. We have demonstrated through simulation that this technique enables, in principle, the imaging of the habitable zone of the Alpha Centauri system. Furthermore, this technique can be combined with the previously discussed super-Nyquist wavefront control (Thomas et al. 2015) to enable operation with a wide range of angular separations between the host stars.

A future paper will provide a laboratory-based demonstration of dark holes generated with SNWC, MSWC, and SNMSWC. Preliminary experimental results are reported in Belikov et al. (2016).

This material is based upon work supported by the National Aeronautics and Space Administration ... DS was supported for part of this work by a NASA Postdoctoral Program fellowship.

REFERENCES

, Abt, H. A. 1983, Ann. Rev. Astr. Ap., 21, 343

Batalha, N. M. et al. 2014, PNAS, 111, 12647

Table 3. Summary of contrast performance and Strehl Ratio (SR) from closed-loop wavefront control simulations of the Alpha Centauri system, for both the near-side dark hole (both without and with MSWC) and the far-side dark hole (using SNMSWC).

Target Stars	Simulation Description	Aberrations	Contrast	SR
α Cen A	0.35m, monochromatic, before EFC, no coronagraph	0nm	7.1×10^{-3}	1.00
α Cen A	0.35m, monochromatic, before EFC, coronagraph	0nm	1.9×10^{-5}	1.00
α Cen A	0.35m, monochromatic, before EFC, coronagraph	32nm	1.9×10^{-5}	0.99
α Cen B	0.35m, monochromatic, before EFC, coronagraph	32nm	1.2×10^{-5}	0.99
α Cen AB	0.35m, monochromatic, before EFC, coronagraph	32nm	3.1×10^{-5}	0.99
α Cen A	0.35m, monochromatic, after EFC without MSWC, coronagraph	32nm	1.5×10^{-10}	0.97
α Cen B	0.35m, monochromatic, after EFC without MSWC, coronagraph	32nm	5.4×10^{-5}	0.97
α Cen AB	0.35m, monochromatic, after EFC without MSWC, coronagraph	32nm	5.4×10^{-5}	0.97
α Cen A	0.35m, monochromatic, after EFC with MSWC, coronagraph	32nm	3.2×10^{-10}	0.92
α Cen B	0.35m, monochromatic, after EFC with MSWC, coronagraph	32nm	1.6×10^{-9}	0.92
α Cen AB	0.35m, monochromatic, after EFC with MSWC, coronagraph	32nm	1.9×10^{-9}	0.92
α Cen AB	0.35m, broadband, before EFC, coronagraph	32nm	3.3×10^{-5}	0.99
α Cen AB	0.35m, broadband, after EFC with MSWC, coronagraph	32nm	8.3×10^{-9}	0.81
α Cen AB	0.35m, broadband, before EFC, coronagraph	32nm	2.1×10^{-5}	0.99
α Cen AB	0.35m, broadband, after EFC with SNMSWC, coronagraph	32nm	8.4×10^{-9}	0.81
α Cen AB	2.4m, monochromatic, after EFC with SNMSWC, coronagraph, SN for A	32nm	3.2×10^{-9}	0.83
α Cen AB	2.4m, monochromatic, after EFC with SNMSWC, coronagraph, SN for A & B	32nm	1.0×10^{-8}	0.68

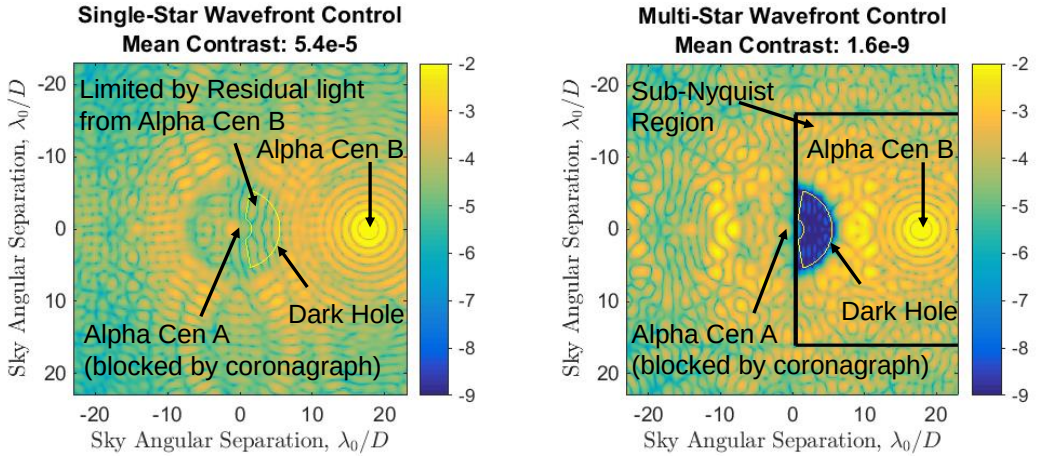

Figure 5. Simulated multi-star dark hole in 650nm monochromatic light for the Alpha Centauri system with a relatively close angular separation of 17.5 λ/D between the binary stars due to a small aperture telescope ($D = 0.35$m): (*Left*) Using EFC around Alpha Centauri A only (the on-axis star blocked by the coronagraph), contrast in the dark hole is ultimately limited by speckles from Alpha Centauri B (the off-axis star in this configuration). (*Right*) Applying EFC with MSWC, leakage from both the central star and the off-axis star can be simultaneously removed. The sub-Nyquist control region for Alpha Centauri B is indicated.

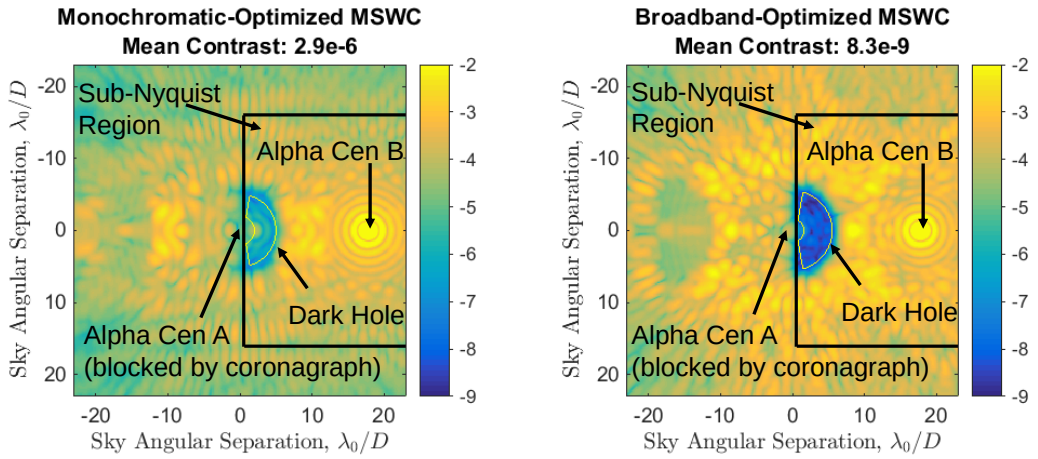

Figure 6. Simulated multi-star dark hole in broadband light featuring a 10% bandwidth around 650nm for the Alpha Centauri system with a relatively close angular separation of 17.5 λ/D between the binary stars due to a small aperture telescope ($D = 0.35$m): (*Left*) Using monochromatic-optimized wavefront control the mean contrast in the dark hole is limited by chromatic effects at 2.9×10^{-6} (*Right*) Applying broadband-optimized wavefront control at three different wavelengths spanning the broadband bandwidth chromatic effects are controlled and a mean contrast of 8.3×10^{-9} is obtained across the dark hole.

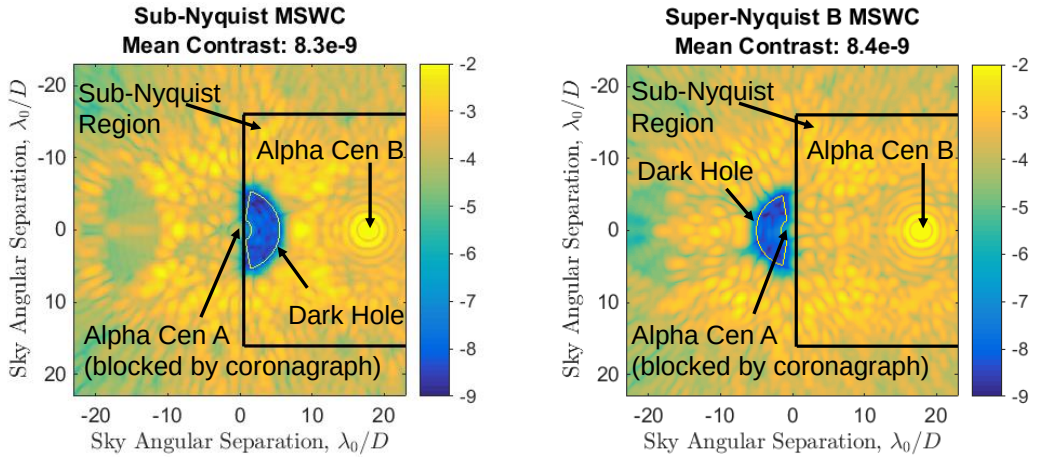

Figure 7. Simulated multi-star dark hole in broadband light with a 10% bandwidth around 650nm for the Alpha Centauri system with a relatively close angular separation of 17.5 λ/D between the binary stars due to a small aperture telescope ($D = 0.35$m). The sub-Nyquist control region for Alpha Centauri B, the off-axis star, is bounded within the indicated square. (*Left*) Multi-Star Wavefront Control is used to generate a dark zone with a mean contrast of 8.3×10^{-9} within the sub-Nyquist region for both Alpha Centauri A and B. (*Right*) Super Nyquist Multi-Star Wavefront Control is used to generate a dark zone in the sub-Nyquist region of Alpha Centauri A and within the Super-Nyquist region for Alpha Centauri B with a mean contrast of 8.4×10^{-9}.

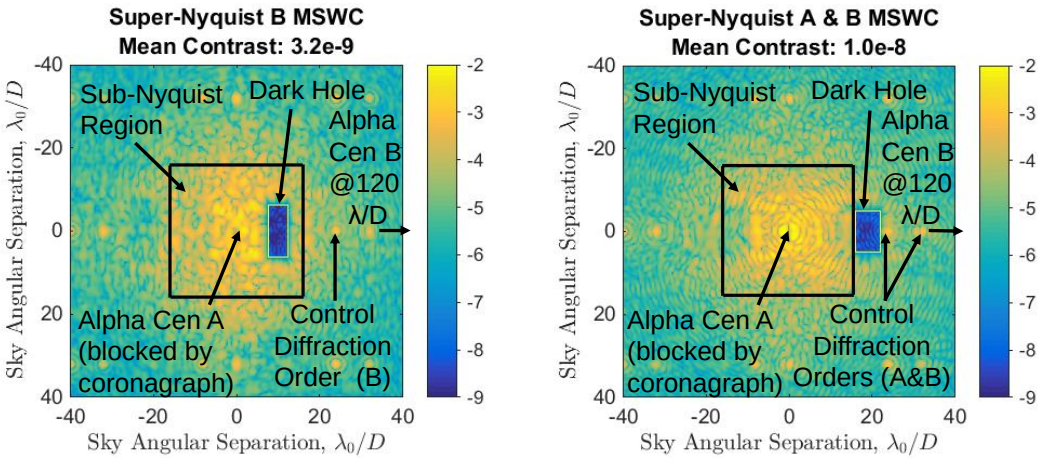

Figure 8. Simulated multi-star dark hole in monochromatic light at 650nm for the Alpha Centauri system with a wider angular separations of 120 λ/D between the binary stars due to a larger aperture telescope ($D = 2.4$m). The sub-Nyquist control region for Alpha Centauri A, the on-axis star, is bounded within the indicated square. (*Left*) Super-Nyquist Multi-Star Wavefront Control is used to generate a dark zone with a mean contrast of 3.2×10^{-9} with the dark zone within the sub-Nyquist region for Alpha Centauri A and within the Super-Nyquist region with respect to Alpha Centauri B. (*Right*) Super-Nyquist Multi-Star Wavefront Control is used to generate a dark zone with a mean contrast of 1.0×10^{-8} at Super-Nyquist separations with respect to both Alpha Centauri A and B. The corresponding diffraction orders used to generate the dark zone are located at $32\lambda/D$ and $24\lambda/D$ respectively and clearly visible as indicated.

Bechter, E. B. et al. 2014, ApJ, 788, 1

Belikov, R. et al. 2015, ArXiv e-print

Belikov, R. et al. 2016, Proc. SPIE, 9904, 990422

Bendek, E., Belikov, R., Pluzhnik, E., and Guyon, O. 2013, PASP, 125, 204

Beuzit, J. L. et al. 2008, Proc. SPIE, 7014, 701418

Bolcar, M. et al. 2016, Proc. SPIE, 9904, 99040J

Borucki, W. J. et al. 2010, Science, 327, 977

Burke, C. J. et al. 2015, ApJ, 809, 1

Cady, E. J., McElwain, M., Kasdin, N. J., Thalmann, C. 2011, PASP, 123, 333

Cady, E. J., et al. 2016, JATIS, 2, 1

Des Marais et al. 2002, Astrobiology, 2, 153.

Duchene, G. 2010, ApJL, 709, 2

Anglada-Escude, G. et al. 2016, Nature, 536, 7617

Give'on, A., Belikov, R., Shaklan, S. B., & Kasdin, N. J. 2007, OExpr, 15, 12338

Give'on, A., Kern, B. D., & Shaklan, S. B.2011, Proc. SPIE, 8151, 815110

Guyon, O. 2003, A&A, 404, 1

Guyon, O. et al. 2010, Proc. SPIE, 7736, 773624

Holman, M. J., & Wiegert, P. A. 1999, AJ, 621, 117

Kern, B. et al. 2016, JATIS, 2, 1

Kraus, A. L. et al. 2016, AJ ,152, 1

Kopparapu, R. K. et al. 2013, ApJ, 765, 131

Wertheimer, J. G. and Laughlin, G. 2006, AJ, 132, 19955

Macintosh, B. et al. 2014, PNAS, 111, 12661

Mennesson, B. et al. 2016, Proc. SPIE, 9904, 99040L

Pueyo, L. et al. 2011, AOpt, 48, 32

Thomas, S. J., Belikov, R., & Bendek, E. 2015, ApJ, 810, 81

Tokovinin, A. 2014, ApJ, 147, 4

Quarles, B., & Lissauer, J. J. 2016, AJ, 151, 111

Quintana, E. V. et al. 2002, ApJ, 576, 982

Quintana, E. V. et al. 2007, ApJ, 660, 807

Raghavan, D. et al. 2010, ApJS, 190, 1

Seo, B. J., et al. 2016, JATIS, 2, 1

Sirbu, D. et al. 2016, JATIS, 2, 2

Sirbu, D., Pluzhnik, E., & Belikov, R. 2016, Proc. SPIE, 9904, 990466

Shaklan, S. B. et al. 2013, Proc. SPIE 8864, 886415